



1 **Measurement report: Chemical characteristics of PM_{2.5} during typical biomass**

2 **burning season at an agricultural site of the North China Plain**

3 Linlin Liang¹, Guenter Engling^{2,3}, Chang Liu¹, Wanyun Xu¹, Xuyan Liu⁴, Yuan Cheng⁵, Zhenyu
4 Du⁶, Gen Zhang¹, Junying Sun¹, Xiaoye Zhang¹

5 ¹ State Key Laboratory of Severe Weather & Key Laboratory for Atmospheric Chemistry, Chinese
6 Academy of Meteorological Sciences, Beijing 100081, China

7 ² Division of Atmospheric Sciences, Desert Research Institute, Reno, NV 89512, USA

8 ³ Now at: California Air Resources Board, El Monte, CA 91731, USA

9 ⁴ National Satellite Meteorological Center, Beijing 100081, China

10 ⁵ School of Environment, Harbin Institute of Technology, Harbin 150001, China

11 ⁶ National Research Center for Environmental Analysis and Measurement, Beijing 100029 China

12 **Abstract:**

13 Biomass burning (BB) activities are ubiquitous in China, especially in North China, where there is
14 an enormous rural population and winter heating custom. BB tracers (i.e., levoglucosan (LG),
15 mannosan (MN) and potassium (K⁺)), as well as other chemical components were quantified at a
16 rural site (Gucheng, GC) in North China from 15 October to 30 November, during a transition
17 heating season, when the field burning of agricultural residues was becoming intense. The
18 measured daily average concentrations of LG, MN and K⁺ in PM_{2.5} during this study were $0.79 \pm$
19 $0.75 \mu\text{g m}^{-3}$, $0.03 \pm 0.03 \mu\text{g m}^{-3}$ and $1.52 \pm 0.62 \mu\text{g m}^{-3}$, respectively. Carbonaceous components
20 and BB tracers showed higher levels at nighttime than daytime, while secondary inorganic ions
21 were enhanced during daytime. An episode with high levels of BB tracers was encountered at the
22 end of October, 2016, with high LG at $4.37 \mu\text{g m}^{-3}$. Based on the comparison of chemical
23 components during different BB pollution periods, it appeared that biomass combustion can
24 obviously elevate carbonaceous components levels, whereas no essentially effect on secondary
25 inorganic aerosols in the ambient air. Moreover, the LG/MN ratios during different BB pollution
26 periods remained at high values (in the range of 18.3-24.9), however, the LG/K⁺ ratio was
27 significantly elevated during the intensive BB pollution period (1.67) when air temperatures
28 decreasing, substantially higher than in other BB periods (averaged at 0.47).



29 **Keywords:** Biomass burning; Organic tracers; Levoglucosan; Mannosan; Potassium

30 **1. Introduction**

31 Particulate air pollution is attracting more and more concerns in China because of their
32 obvious adverse impact on visibility reduction, as well as health implication and regional or global
33 climate change (Kanakidou et al., 2009; Pope and Dockery, 2006; Chen et al., 2017).
34 Carbonaceous species, i.e., organic carbon (OC) and elemental carbon (EC), and water-soluble
35 inorganic ions, e.g., SO_4^{2-} , NO_3^- and NH_4^+ are the major components of ambient aerosols (Liang
36 et al., 2017; Du et al., 2014; Zheng et al., 2015; Tan et al., 2016). Biomass burning emissions
37 constitute a large source of ambient particulate pollution, especially for carbonaceous components,
38 i.e., primary organic carbon (POC) and black carbon (BC) on global scale (Bond et al., 2004; Tang
39 et al., 2018; Salma et al., 2017; Titos et al., 2017). As an important aerosol component, black
40 carbon from industrial and combustion emissions contributes to the enhanced $\text{PM}_{2.5}$ mass
41 concentrations and influences regional radiative forcing (Chen et al., 2017). Fresh biomass
42 burning aerosol was found to be mainly comprised of carbonaceous species which typically
43 constitutes 50-60% of the total particle mass (Hallquist et al., 2009). Yao et al. (2016) identified
44 approximately half of carbonaceous aerosols being contributed by biomass burning at Yucheng, a
45 rural site in the North China Plain.

46 Biomass burning emissions also represent a potentially large source of secondary organic
47 aerosol (SOA). The precursors and formation pathways of SOA from biomass burning emissions
48 were investigated by extensive field observations (e.g., Zhu et al., 2015; 2016; 2017; Adler et al.,
49 2011; Zhang et al., 2010; 2015). Based on morphological particle analysis, Yao et al. (2016)
50 investigated the smoke emitted from biomass burning impacting SOA production. Sun et al. (2010)
51 found that phenolic compounds, which were emitted in large amounts from wood combustion, can
52 form SOA at high yields in aqueous-phase reactions. In addition, smoke from biomass burning can
53 be transported thousands of kilometers downwind from the source areas. Biomass burning aerosol
54 from Southeast Asia can be transported to China, Singapore and even further to North America
55 (Liang et al., 2017; Hertwig et al., 2015; Peltier et al., 2008). Based on molecular tracer
56 measurements, synoptic data as well as air mass back trajectory analysis, a fire episode was



57 captured at a background site of East China with smoke advected from Southeast Asia (Liang et
58 al., 2017).

59 The North China Plain (NCP) is one of the most polluted regions in China. Severe haze–fog
60 of longer duration and more extensive coverage has occurred frequently in the NCP area,
61 especially during the seasons of autumn and winter. NCP covers one quarter of China's cultivated
62 land and yields 35% of the agricultural products in China (Boreddy et al., 2017). The rural
63 population in NCP is also large and dense, and biomass burning activities are common in this
64 region in form of cooking and heating. Intense fire activity typically occurs in October after the
65 corn harvest. Abundant smoke is emitted from agricultural burning, i.e., residential biofuel
66 combustion, open field burns, etc. Various field observations have investigated different aspects of
67 biomass burning, e.g., seasonal variations, chemical and physical properties of smoke particles,
68 spatial distribution, sources, transport, etc., in the NCP region (Cheng et al., 2013; Shen et al.,
69 2018; Sun et al., 2013; 2016; Boreddy et al., 2017; Yan et al., 2015). However, these field
70 investigations of the contribution of biomass burning to ambient aerosols in the NCP region were
71 concentrated on the city of Beijing (Cheng et al., 2013; Zheng et al., 2015; Duan et al., 2004).
72 Little field research about biomass burning was reported for rural areas in the NCP. In fact,
73 biomass burning activities are common in the rural areas of the NCP region, and the resulting
74 smoke aerosol can be transported to urban areas, e.g., the city of Beijing, resulting in haze
75 episodic events. Meanwhile, biomass burning studies at rural sites can provide valuable source
76 information of the biomass burning pollution in the North China region.

77 The objective of this study is to gain insights about the abundance of smoke during the
78 typical biomass burning season, i.e., autumn–winter transition season, following the corn harvest.
79 In this paper, we focus on quantifying multiple biomass burning tracers, i.e., LG, MN and K⁺ as
80 well as other chemical species in PM_{2.5} in Gucheng (GC) during the typical biomass burning
81 season. The results of this study demonstrated the biomass burning pollution status in the rural
82 atmosphere of North China, as well as chemical properties of ambient aerosols under different
83 biomass burning pollution levels.

84



85 2. Site description and experimental Methods

86 2.1 Site description and sampling

87 Samples were collected at a rural site, Gucheng (GC, 39°09'N, 115°44'E; 15.2 m a.s.l),
88 located on a platform at the China Meteorological Administration farm in the town of Gucheng
89 (GC site), approximately 110 km southwest of Beijing and 35 km north of the city of Baoding
90 (population of about 5 million) in Hebei province, as shown in *Figure S1*. The station is
91 surrounded by agricultural fields, with major crop species being corn and wheat. The dominant
92 wind direction at GC is southwest and northeast during the study period. This site is upwind of
93 Beijing, when the wind blows from the south or southwest, where heavily polluted cities and
94 regions of Hebei province, i.e., Baoding, Shijiazhuang, Xingtai, Handan, are located. Thus, it is an
95 appropriate station for representing the air pollution situation in the NCP region (Sheng et al.,
96 2018; Chi et al., 2018; Xu et al., 2019; Kuang et al., 2020).

97 Daytime and nighttime PM_{2.5} samples were collected from 15 October, 2016 to 23 November,
98 2016, by using PM_{2.5} High-volume (Hi-Vol) samplers (GUV-15HBL1, Thermo Fisher Scientific
99 CO., LTD), at the nominal flow rate of 1.13 m³ min⁻¹. The daytime samples were collected from
100 07:00 to 19:00, while nighttime samples were collected from 19:00 to 07:00 local time of the next
101 day. All PM_{2.5} samples were collected on quartz fiber filters, prebaked at 850 °C for at least 5 h to
102 remove carbonaceous material. A total of 33 couples of daytime/nighttime samples and 6
103 whole-day samples as well as 4 field blank samples were collected during the sampling period.
104 The filters were stored at -20 °C after sample collection.

105 2.2 Experimental Methods

106 2.2.1 Anhydrosugar and water-soluble inorganic ion analysis

107 The quartz filter samples were analyzed for biomass burning anhydrosugar tracers, i.e., LG
108 and MN, using an improved high-performance anion-exchange chromatography (HPAEC) method
109 with pulsed amperometric detection (PAD) on a Dionex ICS-5000+ system. LG and MN were
110 separated by a Dionex Carbopac MA1 analytical column and guard column with an aqueous
111 sodium hydroxide (NaOH, 480 mM) eluent at a flow rate of 0.4 mL min⁻¹. The detection limit of
112 LG and MN was 0.002 mg L⁻¹ and 0.005 mg L⁻¹, respectively. More details about the



113 HPAEC-PAD method can be found elsewhere (Iinuma et al., 2009).

114 The quartz filter samples were also analyzed for water-soluble inorganic ions by a Dionex
115 ICS-5000+ ion chromatograph, including three anions (i.e., SO_4^{2-} , NO_3^- , Cl^-) and five cations
116 (i.e., NH_4^+ , Ca^{2+} , Na^+ , K^+ and Mg^{2+}). The cations were separated on an Ionpac CS12 analytical
117 column and CG12 guard column with a 20 mM methanesulphonic acid as eluent at a flow rate of
118 1.0 mL min^{-1} , while the anions were separated on an Ionpac AS11-HC column and AG11-HC
119 guard column with 21.5 mM KOH eluent at a flow rate of 1.0 mL min^{-1} . The water-soluble
120 inorganic ion data were corrected by field blanks.

121 **2.2.2 Organic carbon/elemental carbon analysis**

122 OC and EC were measured on a punch (0.526 cm^2) of each quartz sample by a
123 thermal/optical carbon analyzer (DRI Model 2001, Desert Research Institute, USA), using the
124 Interagency Monitoring of Protected Visual Environments (IMPROVE) thermal evolution
125 protocol with reflectance charring correction. The analytical error of OC was within 10%, and one
126 sample of every 10 samples was selected at random for duplicate analysis. The detection limit of
127 OC was $0.82 \mu\text{gC cm}^{-2}$ (Liang et al., 2017).

128 **2.2.3 Gas online monitoring (i.e., NO, NO₂, SO₂, O₃, CO and NH₃)**

129 During this campaign, commercial instruments from Thermo Fisher Scientific Co., LTD were
130 used to measure O_3 (TE 49C), $\text{NO}/\text{NO}_2/\text{NO}_x$ (Model 42CTL), CO (TE 48CTL), and SO_2
131 (TE43CTL), while NH_3 was measured by an ammonia analyzer (DLT-100, Los Gatos Research,
132 USA) at GC station. All measurement data quality was controlled according to standard gases (Xu
133 et al., 2019; Lin et al., 2011; Meng et al., 2018; Ge et al., 2018).

134 **2.2.4 Meteorological parameters**

135 The meteorological parameters, including air temperature, relative humidity (RH) and wind
136 speed at a 24-h resolution at the GC site are presented in Figure 1. During this campaign, the daily
137 average RH value was observed at $77 \pm 13\%$, with a range from 48% to 99%, while the daily wind
138 speed was observed with an average value of $1.07 \pm 1.14 \text{ m s}^{-1}$, exhibiting moist and stable
139 synoptic conditions at this rural site during the autumn-winter transition season. During the
140 sampling time from 15 October, 2016 to 23 November, 2016, the mean RH at GC was observed at
141 77%, exhibiting moist conditions. These meteorological parameters indicate that GC was



142 characterized by humid and stagnant air masses. Moreover, there was rare precipitation during the
143 sampling period at the GC site, except for two days, i.e., 20 and 27 October, 2016 (Figure 1).

144 **2.2.5 Back trajectory and fire spot analysis**

145 To characterize the transport pathways of the aerosol at the Gucheng site, back-trajectories
146 were calculated with the NOAA Hybrid Single-Particle Lagrangian Integrated Trajectory
147 (HYSPLIT) model via NOAA ARL READY Website (<http://ready.arl.noaa.gov/HYSPLIT.php>).

148 To investigate the influence of biomass burning activities in surrounding areas, fire hot spot
149 counts were obtained from the Fire Information for Resource Management System (FIRMS)
150 (available at <https://firms.modaps.eosdis.nasa.gov/download/>).

151 **3. Results and discussion**

152 **3.1 Characteristics of chemical components in PM_{2.5}**

153 In this study, the mass concentration of PM_{2.5-cal} was reconstituted by the sum of carbonaceous
154 components (1.6×OC + EC) and inorganic ions (SO₄²⁻ + NH₄⁺ + NO₃⁻ + Cl⁻ + Ca²⁺ + Na⁺ + K⁺ +
155 Mg²⁺). Figure 1 describes the time-series variation obtained for daily PM_{2.5-cal}, and its major
156 components (OC, EC, SO₄²⁻, NO₃⁻ and NH₄⁺), biomass burning tracers (LG, MN and K⁺) and
157 meteorological factors (temperature (T), relative humidity (RH), wind speed (WS) and rainfall)
158 during the sampling period. The average daily PM_{2.5-cal} mass concentration in the autumn-winter
159 transition season at GC reached 137 ± 72.4 μg m⁻³, ranging from 23.3 μg m⁻³ to 319 μg m⁻³ (Table
160 1), which is higher than during the severe winter haze in January, 2013 at an urban site in Beijing
161 (121.0 μg m⁻³) (Zheng et al., 2015). The mass concentrations of these chemical species during the
162 day are distributed as follows (from highest to lowest): OC > EC > NO₃⁻ > SO₄²⁻ > NH₄⁺ > Cl⁻ >
163 Ca²⁺ > K⁺ > Na⁺ > Mg²⁺. Organic matter (OM) was the most abundant component, the daily
164 average value of which was 70.4 ± 49.6 μg m⁻³, accounting for nearly half (46.7%) of PM_{2.5-cal}
165 mass, indicating obvious organic pollution at the rural site in the North China Plain during the
166 sampling season.

167 The measured daily average concentrations of biomass burning tracers, i.e., LG, MN and K⁺
168 in PM_{2.5} during our study were 0.79 ± 0.75 μg m⁻³, 0.03 ± 0.03 μg m⁻³ and 1.52 ± 0.62 μg m⁻³
169 (Table 1). The anhydrosugar levels (LG and MN) in this study were both higher than those



170 observed in the city of Beijing during summer and winter seasons (Cheng et al., 2013; Yan et al.,
171 2015). The highest concentrations of LG in GC were observed on 31 October, 2016 with $4.37 \mu\text{g m}^{-3}$
172 m^{-3} , which is a sharp increase (over 30 times) of the minimum concentration ($0.14 \mu\text{g m}^{-3}$) during
173 that period. Accordingly, the $\text{PM}_{2.5\text{-cal}}$ concentration during that period was also elevated (as high
174 as $236 \mu\text{g m}^{-3}$) (Figure 1). Secondary inorganic aerosol (sulfate, SO_4^{2-} ; nitrate, NO_3^- and
175 ammonium, NH_4^+ , SNA) species, were the major water soluble ions, accounting for 82.8% of total
176 water soluble ions, the daily average values of which were $10.5 \pm 6.87 \mu\text{g m}^{-3}$, $15.9 \pm 9.29 \mu\text{g m}^{-3}$
177 and $10.9 \pm 5.51 \mu\text{g m}^{-3}$ (Table 1). SNA species exhibited a synchronous temporal trend, while the
178 NO_3^- concentrations exceeded those of SO_4^{2-} at the GC site, in contrast to the results of previous
179 studies, e.g., Tan et al. (2016), who found SO_4^{2-} to be the dominant species in $\text{PM}_{2.5}$ during winter
180 time in 2006 in Beijing. Similarly, Chi et al., (2018) also found NO_3^- concentrations exceeded
181 those of SO_4^{2-} at both Beijing and GC sites during the winter time in 2016, although they observed
182 that NH_4^+ was the dominant component of SNA (the concentrations of SO_4^{2-} , NO_3^- and NH_4^+
183 were $14.0 \mu\text{g m}^{-3}$, $14.2 \mu\text{g m}^{-3}$, and $24.2 \mu\text{g m}^{-3}$, respectively).

184 **3.2 Day-night variations in the characteristics of $\text{PM}_{2.5}$ chemical components**

185 Carbonaceous components and biomass burning tracers exhibited higher levels during
186 nighttime than daytime, while secondary inorganic ions showed the opposite pattern, i.e., higher
187 concentrations during daytime than nighttime (Figure 2 and Figure S2). Besides, the gap of
188 carbonaceous components and anhydrosugars between daytime and nighttime (two-fold) was
189 more significant than for secondary inorganic ions. Elemental carbon and primary organic
190 components are not subject to significant differences in chemical reactions in ambient air between
191 daytime and nighttime, and they will be mainly influenced by the variations of the planetary
192 boundary layer (PBL) height. In the night, the PBL height decreases, compressing air pollutants
193 into a shallow layer, and subsequently resulting in faster accumulation and higher concentrations
194 of pollutants (Zheng et al., 2015; Zhong et al., 2018; 2019). The contributions of OM and EC to
195 $\text{PM}_{2.5\text{-cal}}$ were observed to be higher at nighttime (53.9% and 16.6%) than daytime (43.8% and
196 13.7%) as well (Figure 3). Moreover, the chemical degradation of LG may occur due to
197 photochemical reaction in the ambient aerosols, further lowering the LG levels in daytime (Sang
198 et al., 2016; Gensch et al., 2018). Correspondingly, the contribution of LG to $\text{PM}_{2.5\text{-cal}}$ during



199 nighttime (0.64%) was observed to be higher than that during daytime (0.37%) (Figure 3).
200 However, secondary inorganic ions have an important formation pathway, i.e., photochemical
201 processing, during daytime. Thus, the secondary inorganic species (SO_4^{2-} , NO_3^- and NH_4^+) were
202 enhanced during daytime due to photochemical formation. Moreover, such an enhancement in
203 secondary transformations during daytime is more evident in terms of the mass contributions of
204 secondary inorganic ions to $\text{PM}_{2.5\text{-cal}}$, that the contributions of SO_4^{2-} , NO_3^- and NH_4^+ to $\text{PM}_{2.5\text{-cal}}$
205 decreased from daytime (9.9%, 14.5% and 10.0%) to nighttime (6.5%, 9.6% and 7.1%) (Figure 3).

206 In addition, the concentrations of other water-soluble inorganic ions, i.e., K^+ and Cl^- during
207 nighttime ($1.78 \pm 0.95 \mu\text{g m}^{-3}$ and $6.08 \pm 4.00 \mu\text{g m}^{-3}$) were higher than those in daytime ($1.43 \pm$
208 $0.54 \mu\text{g m}^{-3}$ and $4.33 \pm 2.30 \mu\text{g m}^{-3}$), while their contributions to $\text{PM}_{2.5\text{-cal}}$ were reversed, due to the
209 significant accumulation and higher concentrations of pollutants during nighttime. As Ca^{2+} , Mg^{2+}
210 and Na^+ , mainly emitted from primary natural sources, such as dust, soil resuspension and sea salt,
211 are subject to more activity during the daytime and also influenced by the airflow dynamics, the
212 contribution of those species in nighttime were lower than those during daytime, especially for
213 Ca^{2+} , decreasing from 2.2% in daytime to 0.9% at nighttime (Figure 3).

214 3.3 Biomass burning episodes and the impacts on chemical $\text{PM}_{2.5}$ characteristics

215 An episode with high biomass burning tracer levels was encountered on 31 October, 2016.
216 The concentrations of LG in $\text{PM}_{2.5}$ during this one-day episode ($4.37 \mu\text{g m}^{-3}$) were significantly
217 higher than those during typical transition season at the GC site ($0.69 \pm 0.47 \mu\text{g m}^{-3}$) (Figure 1).
218 Here, we mainly distinguish four sub-periods based on daily LG concentrations during the time
219 frame from 15 October to 23 November, 2016. The four periods were separated as follows: 15-30
220 October (Period I: Minor biomass burning), 31 October (Period II: Intensive biomass burning),
221 1-14 November (Period III: Major biomass burning), 15-23 November (Period IV: Heating
222 season). Table 2 compares the concentrations of $\text{PM}_{2.5\text{-cal}}$ mass, chemical components and gases at
223 the GC site during these four periods, as well as the ratios between the intensive, major BB
224 periods and heating season to minor BB period. The level of LG during the intensive BB episode
225 II was about 12 times of that during the minor BB period I. K^+ and Cl^- , the common biomass
226 burning tracers utilized in many studies (Duan et al., 2004; Cheng et al., 2013), were also
227 observed with increased abundance during intensive BB episode II. When entering into November,



228 the weather was becoming cold, and thus combustion activities for heating in the rural areas
229 commenced, resulting in the ambient levels of LG to strongly increase to $0.92 \pm 0.47 \mu\text{g m}^{-3}$
230 during period III, about 3 times of those in Period I. The central heating systems in North China
231 cities were operated during period IV, and the ambient level of LG was observed at $0.96 \pm 0.63 \mu\text{g}$
232 m^{-3} , which was slightly higher than that in period III.

233 The concentrations of OC and EC were also observed strongly increased in period II (Table 2),
234 especially for OC, increased to $59.9 \pm 25.3 \mu\text{g m}^{-3}$ during the intensive BB episode II, nearly 6
235 times of that during the minor BB period ($16.2 \pm 7.52 \mu\text{g m}^{-3}$). Accordingly, the LG/OC ratio
236 increased to 0.045 during period II, which is higher than most of the published field observations,
237 i.e., at urban sites (Zhang et al., 2008; Cheng et al., 2013; Zhang et al., 2014), rural sites (Sang et
238 al., 2013; Ho et al., 2014; Pietrogrande et al., 2015; Mkoma et al., 2013) and agricultural sites (Ho
239 et al., 2014; Jung et al., 2014), yet lower than at an urban site in northern Italy during winter time
240 (Pietrogrande et al., 2015). During the major BB (period III) and heating season (period IV), due
241 to the combustion of coal and biofuel for heating, OC remained at a high level ($55.2 \pm 17.1 \mu\text{gC}$
242 m^{-3} and $69.4 \pm 24.6 \mu\text{gC m}^{-3}$, respectively). These levels are more than 3 times of that during the
243 minor BB period I. Due to the abundance of organic aerosols, the LG/OC ratios during periods III
244 and IV decreased to 0.016 ± 0.005 and 0.014 ± 0.006 , respectively, even lower than those in the
245 minor BB period I (0.025 ± 0.008).

246 Compared to the carbonaceous components, the concentrations of secondary inorganic
247 aerosol species (SO_4^{2-} , NO_3^- , NH_4^+) exhibited a different pattern, i.e., showing no obvious
248 differences between minor BB period I and other three periods. The ratios of SO_4^{2-} , NO_3^- , NH_4^+
249 during periods II, III and IV to period I were all around 1.0 (Table 2), with no increasing trend.
250 Moreover, the relationships between LG and OC (and EC) were better than those between LG and
251 SNA during daytime and nighttime (**Figure S3**). The precursor gases of SNA, i.e., SO_2 , NO, NO_2
252 and NH_3 , were observed to have an increasing trend when biomass burning was prevalent during
253 periods III and IV, with the ratios to period I arranged from 1.13 to 1.90 (Table 2). The time-series
254 variations of the gases (SO_2 , NO_x , NH_3 , CO and O_3) and PBL during the sampling period are
255 shown in **Figure S4**. The primary emission gases were exhibited negative relationships with PBL,
256 while O_3 exhibited obvious positive relationship with PBL (**Figure S5**). Combustion from



257 different fossil fuels (coal, gasoline, diesel, etc.) and biomasses (straws, woods, leaves, etc.) can
258 all emit CO into the atmosphere (Streets et al., 2003; Chantara et al., 2019; Merico et al., 2020).
259 Due to the more abundant combustion in the colder weather, the concentrations of CO also
260 increased to 1.65 ± 0.53 ppm and 1.18 ± 0.83 ppm during the major biomass burning period III
261 and the heating season period IV, respectively.

262 The combustion of biomass, especially of agricultural residues (e.g., wheat and corn straw) is
263 very common in the rural areas in North China during the autumn-winter transition period. During
264 the autumn harvest season in North China, wheat and corn straw burning is common practice,
265 resulting in more abundant fire spots when entering into November than period I (Figure 4). The
266 intense biomass burning event on 31 October, 2016 was also supported by air mass back trajectory
267 analysis (Figure 5), performed with the TrajStat software. Based on the 48 h back trajectories at
268 the GC site at 00:00 (UTC time) on 1 November, 2016, the air mass at the GC site was restricted
269 in the region of Beijing-Tianjing-Hebei, the polluted area where fire spots were numerous.
270 However, on the previous and following day of this episode, i.e., 31 October and 2 November
271 onward, the air masses arriving at GC were advected from the northwest of Mongolia, where
272 mostly desert areas are present, with less farm land and rare biomass burning activities (Figure 5).

273 Mean percentiles of major components in $PM_{2.5}$ with respect to different BB pollution
274 periods at GC site during the sampling time are shown in Figure 6. With the variation of BB
275 pollution periods, the EC fraction seems to exhibit no obvious change during periods I, II and III,
276 but slightly increased during the heating season (period IV), while the OC fraction increased
277 significantly. The contributions of sulfate, nitrate and ammonium to $PM_{2.5-cal}$ all decreased sharply
278 from the minor BB period to the intense period (Figure 6). This suggests that organic aerosol
279 species become more important during BB pollution periods, concerning their contribution to the
280 $PM_{2.5-cal}$, while EC has no such character. The OM percentage during intense BB period II was
281 65.4%, about double of that during the minor biomass burning period (34.0%), indicating that
282 there was a large fraction of OM in $PM_{2.5-cal}$ originating from BB at the GC site during intensive
283 BB period II. Opposite to OM, contributions of secondary inorganic ions to $PM_{2.5-cal}$ significantly
284 decreased with the BB pollution becoming more severe. The contributions of SO_4^{2-} , NO_3^- and
285 NH_4^+ to $PM_{2.5-cal}$ during the minor BB episode (11.6%, 20.5% and 12.5%) obviously declined



286 during the intense BB episode (1.73%, 7.73% and 4.24%).

287 **3.4 Relationships among tracers during different biomass burning pollution** 288 **periods**

289 In addition to pollution level information of biomass burning molecular tracers, the ratios
290 between them could also be used to identify the different biomass types or indicate the burning
291 formation processes of atmospheric aerosols. The LG/MN ratios during minor, intense, major
292 biomass pollution and heating season periods were observed at high values, i.e., 24.9, 24.1, 24.8
293 and 18.3 respectively (Table 2, Figure 7). LG and MN in the four periods showed a good
294 relationship (Figure 7a, $R^2 = 0.94$). Based on source emission studies, the LG/MN ratios from crop
295 residue burning, i.e., rice straw, wheat straw, and other straws, were similar and characterized by
296 high values, yet overlapped with those from hard wood and leaf burning (>10.0), while soft wood
297 characterized by relatively lower LG/MN ratios (< 5.0) (Cheng et al., 2013). According to the
298 local habits, woods are also commonly used as biofuels for stove heating in North China, since
299 they allow long-time heating duration. The influence of wood combustion for heating becoming
300 non-negligible during the cold season caused the LG/MN ratios during the intense BB episode
301 (Period II) and typical heating season (Period IV) to slightly decrease.

302 The concentrations of LG and K^+ during minor, major BB episode and heating season were
303 correlated well (Figure 7b, $R^2 = 0.70$), while the red dot of period II being off from the fitted
304 regression line. The LG/ K^+ ratios during III and IV (0.52 and 0.53) were similar to those during a
305 BB episode at an urban site of Beijing during winter time (LG/ $K^+ = 0.51$) (Cheng et al., 2013).
306 However, the LG/ K^+ ratio during the intense BB period II increased to 1.67, which was
307 significantly higher than that in typical straw combustion (< 1.0). Correspondingly, there was a
308 significant drop in temperatures at the GC site during period II, with the average daily temperature
309 sharply decreasing from 7.5 °C on 30 Oct to 0.31 °C on 31 Oct, 2016, while the average
310 temperature at night of 31 Oct decreased to -3.4 °C (Figure 1). Hence, the combustion activities
311 were apparently intense around the sampling site for heating purposes. Compared to K^+ , there is a
312 large enrichment of LG in wood burning emissions, based on the results from previous biomass
313 source combustion studies (Engling et al., 2006; Chantara et al., 2019). The influence of softwood



314 and/or other materials from softwood, which are commonly used as biofuels for stove heating in
315 North China (Sang et al., 2012; Cheng et al., 2013; Zhou et al., 2017), should be larger during this
316 low temperature period. Moreover, LG/K^+ ratios also can be influenced by combustion conditions,
317 i.e., smoldering versus flaming burns. Biofuels are typically subject to smoldering combustion
318 condition in residential stoves for heating purposes in the rural areas in North China, which was
319 reflected in relatively higher LG/K^+ ratios than during flaming combustion (Schkolnik et al., 2005;
320 Lee et al., 2010).

321 **4. Summary and conclusion**

322 Anhydrosugars, including levoglucosan and mannosan, and water-soluble potassium ion
323 were employed as molecular tracers to investigate the characteristics of biomass burning activities
324 as well as chemical properties of ambient aerosols under different biomass burning pollution
325 levels. The measured daily average concentrations of LG, MN and K^+ in $PM_{2.5}$ during a typical
326 biomass burning season, from 15 October to 30 November, 2016 were $0.79 \pm 0.75 \mu\text{g m}^{-3}$, $0.03 \pm$
327 $0.03 \mu\text{g m}^{-3}$ and $1.52 \pm 0.62 \mu\text{g m}^{-3}$. The concentrations of carbonaceous components and biomass
328 burning tracers were observed higher at nighttime than daytime, while the patterns of secondary
329 inorganic ions (SO_4^{2-} , NO_3^- and NH_4^+) were opposite, since they were enhanced by photochemical
330 formation during daytime. An episode with extreme biomass burning tracer levels was
331 encountered on 31 October, 2016, with concentrations of LG as high as $4.37 \mu\text{g m}^{-3}$. Comparing
332 the chemical composition between different biomass burning periods, it was apparent that biomass
333 burning can considerably elevate the levels of organic components, while not showing a
334 significant effect on the production of secondary inorganic ions, although their precursors were
335 observed at increased levels. Moreover, due to more local soft wood and smoldering combustion
336 taking place for heating under the low temperatures, the LG/K^+ ratio during the intensive BB
337 period was abnormally higher than those in other BB periods.

338

339 **Data availability.** The data used in this study can be obtained from this open link:
340 <https://pan.baidu.com/s/11bKUZff1KJbzNVxS3VsLaA> code: jvqx. It is also available from the
341 corresponding author upon request (lianglinlin@cma.gov.cn).

342 **Author contributions.** LL designed conducted all observations and drafted the paper. GE revised



343 the paper and improved the English writing. XL drew the Figure 4 and Figure 5. CL, WX, YC, ZD,
344 GZ, JS and XZ interpreted the data and discussed the results. All authors approved the final
345 version for publication.

346 **Competing interests.** The authors declare that they have no conflict of interest.

347 **Special issue statement.** This article is part of the special issue “In-depth study of air pollution
348 sources and processes within Beijing and its surrounding region (APHH-Beijing) (ACP/AMT
349 interjournal SI)”. It is not associated with a conference.

350 **Acknowledgements.** This research is supported by the Beijing Natural Science Foundation
351 (8192055) and CAMS Fundamental Research Funds (No. 2017Z011). The authors would like to
352 acknowledge Yingli Yu and Ye Kuang for their help with PM_{2.5} samples collection; Hongbing
353 Cheng for help with chemical analyses.

354 **Financial support.** This research has been supported by the Beijing Natural Science Foundation
355 (No. 8192055), State Environmental Protection Key Laboratory of Sources and Control of Air
356 Pollution Complex (No. SCAPC201701) and Chinese Academy of Meteorological Sciences
357 Fundamental Research Funds (No. 2017Z011).

358 **References:**

- 359 Boreddy, S. K. R., Kawamura, K., Okuzawa, K., Kanaya, Y., and Wang, Z.: Temporal and diurnal
360 variations of carbonaceous aerosols and major ions in biomass burning influenced aerosols
361 over Mt. Tai in the North China Plain during MTX2006, *Atmos. Environ.*, 154, 106-117,
362 <http://dx.doi.org/10.1016/j.atmosenv.2017.01.042>, 2017.
- 363 Caseiro, A., Bauer, H., Schmidl, C., Pio, C. A., and Puxbaum, H.: Wood burning impact on PM₁₀
364 in three Austrian regions, *Atmos. Environ.*, 43, 2186-2195,
365 <https://doi.org/10.1016/j.atmosenv.2009.01.012>, 2009.
- 366 Chantara, S., Thepnuan, D., Wiriyaa, W., Prawan, S., and Tsai, Y.I.: Emissions of pollutant gases,
367 fine particulate matters and their significant tracers from biomass burning in an open-system
368 combustion chamber, *Chemos.* 224, 407-416,
369 <https://doi.org/10.1016/j.chemosphere.2019.02.153>, 2019.
- 370 Chen, J., Li, C., Ristovski, Z., Milic, A., Gu, Y., Islam, M. S., Wang, S., Hao, J., Zhang, H., He, C.,
371 Guo, H., Fu, H., Miljevic, B., Morawska, L., Thai, P., Lam, Y. F., Pereira, G., Ding, A.,
372 Huang, X., and Dumka, U. C.: A review of biomass burning: Emissions and impacts on air
373 quality, health and climate in China, *Sci. Tot. Environ.*, 579, 1000-1034,
374 <https://doi.org/10.1016/j.scitotenv.2016.11.025>, 2017.
- 375 Cheng, Y., Engling, G., He, K.B., Duan, F.K., Ma, Y.L., Du, Z.Y., Liu, J.M., Zheng, M., and Weber,
376 R.J.: Biomass burning contribution to Beijing aerosol, *Atmos. Chem. Phys.*, 13, 7765-7781,
377 <https://doi.org/10.5194/acp-13-7765-2013>, 2013.
- 378 Chi, X., He, P., Jiang, Z., Yu, X., Yue, F., Wang, L., Li, B., Kang, H., Liu, C., and Xie, Z.: Acidity
379 of aerosols during winter heavy haze events in Beijing and Gucheng, China, *J. Meteorol. Res.*,



- 380 32, 14-25, <https://doi.org/10.1007/s13351-018-7063-4>, 2018.
- 381 Drewnick, F., Hings, S. S., Curtius, J., Eerdekens, G., and Williams, J.: Measurement of fine
382 particulate and gas-phase species during the New Year's fireworks 2005 in Mainz, Germany,
383 *Atmos. Environ.*, 40, 4316-4327, <https://doi.org/10.1016/j.atmosenv.2006.03.040>, 2006.
- 384 Du, Z.Y., He, K.B., Cheng, Y., Duan, F.K., Ma, Y. L., Liu, J.M., Zhang, X.L., Zheng, M., and
385 Weber, R.: A yearlong study of water-soluble organic carbon in Beijing I: Sources and its
386 primary vs. secondary nature, *Atmos. Environ.*, 92, 514-521,
387 <https://doi.org/10.1016/j.atmosenv.2014.04.060>, 2014.
- 388 Duan, F., Liu, X., Yu, T., and Cachier, H.: Identification and estimate of biomass burning
389 contribution to the urban aerosol organic carbon concentrations in Beijing, *Atmos. Environ.*,
390 38, 1275-1282, <https://doi.org/10.1016/j.atmosenv.2003.11.037>, 2004.
- 391 Engling, G., Carrico, C.M., Kreidenweis, S.M., Collett Jr, J.L., Day, D.E., Malm, W.C., Lincoln,
392 L., Hao, W.M., Iinuma, Y., and Herrmann, H.: Determination of levoglucosan in biomass
393 combustion aerosol by high-performance anion-exchange chromatography with pulsed
394 amperometric detection, *Atmos. Environ.*, 40, S299-S311,
395 <https://doi.org/10.1016/j.atmosenv.2005.12.069>, 2006.
- 396 Engling, G., Lee, J. J., Tsai, Y. W., Lung, S. C. C., Chou, C. C. K., and Chan, C. Y.: Size resolved
397 anhydrosugar composition in smoke aerosol from controlled field burning of rice straw,
398 *Aerosol Sci. Tech.*, 43, 662-672, <https://doi.org/10.1080/02786820902825113>, 2009.
- 399 Ge, B.Z., Wang, Z.F., Lin, W.L., Xu, X.B., Li, J., Ji, D.S., and Ma, Z.Q.: Air pollution over the
400 north china plain and its implication of regional transport: a new sight from the observed
401 evidences, *Environ. Pollut.*, 166, 29-38, <https://doi.org/10.1016/j.envpol.2017.10.084>, 2017.
- 402 Gensch, I, Sang-Arlt, X.F, Laumer, W, Chan, C.Y, Engling, G, Rudolph, J., and Kiendler-Scharr,
403 A.: Using $\delta^{13}\text{C}$ of levoglucosan as a chemical clock, *Environ. Sci. Tech.*
404 <https://pubs.acs.org/doi/10.1021/acs.est.8b03054>, 2018.
- 405 He, K.B., Zhao, Q., Ma, Y.L., Duan, F.K., Yang, F.M., Shi, Z.B., and Chen, G.: Spatial and
406 seasonal variability of PM_{2.5} acidity at two Chinese megacities: insights into the formation
407 of secondary inorganic aerosols, *Atmos. Chem. Phys.*, 12, 1377-1395,
408 <https://doi.org/10.5194/acp-12-1377-2012>, 2012.
- 409 Hertwig, D., Burgin, L., Gan, C., Hort, M., Jones, A., Shaw, F., Witham, C., and Zhang, K.:
410 Development and demonstration of a Lagrangian dispersion modeling system for real-time
411 prediction of smoke haze pollution from biomass burning in Southeast Asia, *J. Geophys. Res.*:
412 *Atmos.*, 120, 12605-12630, <https://doi.org/10.1002/2015JD023422>, 2015.
- 413 Ho, K.F., Engling, G., Sai Hang Ho, S., Huang, R., Lai, S., Cao, J., and Lee, S.C.: Seasonal
414 variations of anhydrosugars in PM_{2.5} in the Pearl River Delta Region, China, *Tellus B*, 66,
415 22577, <https://doi.org/10.3402/tellusb.v66.22577>, 2014.
- 416 Jung, J., Lee, S., Kim, H., Kim, D., Lee, H., and Oh, S.: Quantitative determination of the
417 biomass-burning contribution to atmospheric carbonaceous aerosols in Daejeon, Korea,
418 during the rice-harvest period, *Atmos. Environ.*, 89, 642-650,
419 <https://doi.org/10.1016/j.atmosenv.2014.03.010>, 2014.
- 420 Kanakidou, M., Seinfeld, J. H., Pandis, S. N., Barnes, I., Dentener, F. J., Facchini, M. C., Van
421 Dingenen, R., Ervens, B., Nenes, A., Nielsen, C. J., Swietlicki, E., Putaud, J. P., Balkanski, Y.,
422 Fuzzi, S., Horth, J., Moortgat, G. K., Winterhalter, R., Myhre, C. E. L., Tsigaridis, K., Vignati,
423 E., Stephanou, E. G., and Wilson, J.: Organic aerosol and global climate modelling: a review,
424 *Atmos. Chem. Phys.*, 5, 1053-1123, <https://doi.org/10.5194/acp-5-1053-2005>, 2005.
- 425 Klejnowski, K., Janoszka, K., and Czaplicka, M.: Characterization and seasonal variations of
426 organic and elemental carbon and levoglucosan in PM₁₀ in Krynica Zdroj, Poland, *Atmos.*,
427 8(10), 190. <https://doi.org/10.3390/atmos8100190>, 2017.



- 428 Kuang, Y., Xu, W.Y., Lin, W.L., Meng, Z.Y., Zhao, H. R., Ren, S.X. Zhang, G., Liang, L. L., and
429 Xu, X. B.: Explosive morning growth phenomena of NH₃ on the North China Plain: Causes
430 and potential impacts on aerosol formation, *Environ. Pollut.*,
431 <https://doi.org/10.1016/j.envpol.2019.113621>, in press, 2020.
- 432 Lee, T., Sullivan, A.P., Mack, L., Jimenez, J.L., Kreidenweis, S.M., Onasch, T.B., Worsnop, D.R.,
433 Malm, W., Wold, C.E., Hao, W.M., and Collett Jr., J.L.: Chemical smoke marker emissions
434 during flaming and smoldering phases of laboratory open burning of wildland fuels, *Aerosol
435 Science and Technology* 44. <http://dx.doi.org/10.1080/02786826.2010.499884>, 2010.
- 436 Lin, W.L., Xu, X.B., Sun, J.Y., Liu, X.W., and Wang, Y.: Background concentrations of reactive
437 gases and the impacts of long-range transport at the jinsha regional atmospheric background
438 station, *Science China (Earth Sciences)*, 54, 1604-1613, 2011.
- 439 Liu, L., Liu, Y., Wen, W., Liang, L., Ma, X., Jiao, J., and Guo, K.: Source Identification of Trace
440 Elements in PM_{2.5} at a Rural Site in the North China Plain, *Atmos.*, 11(2), 179,
441 <https://doi.org/10.3390/atmos11020179>, 2020.
- 442 Meng, Z.Y., Xu, X.B., Lin, W. L., Ge, B.Z., Xie, Y.L., Song, B., Jia, S.H., Zhang, R., Peng, W.,
443 Wang, Y., Cheng, H.B., Yang, W., and Zhao, H.R.: Role of ambient ammonia in particulate
444 ammonium formation at a rural site in the North China Plain, *Atmos. Chem. Phys.*, 18, 167–
445 184, <https://doi.org/10.5194/acp-18-167-2018>, 2018.
- 446 Merico, E., Grasso, F.M., Cesari, D., Decesari, S., Belosi, F., Manarini, F., De Nuntiis, P.,
447 Rinaldi, M., Gambaro, A., Morabito, E., and Contini, D.: Characterisation of atmospheric
448 pollution near an industrial site with a biogas production and combustion plant in southern
449 Italy, <https://doi.org/10.1016/j.scitotenv.2020.137220>, *Sci. Tot. Environ.*, 717, 137220, 2020.
- 450 Mkoma, S. L., Kawamura, K., and Fu, P. Q.: Contributions of biomass/biofuel burning to organic
451 aerosols and particulate matter in Tanzania, East Africa, based on analyses of ionic species,
452 organic and elemental carbon, levoglucosan and mannosan, *Atmos. Chem. Phys.*, 13, 10325–
453 10338, <https://doi.org/10.5194/acp-13-10325-2013>, 2013.
- 454 Peltier, R. E., Hecobian, A. H., Weber, R. J., Stohl, A., Atlas, E. L., Riemer, D. D., Blake, D. R.,
455 Apel, E., Campos, T., and Karl, T.: Investigating the sources and atmospheric processing of
456 fine particles from Asia and the Northwestern United States measured during INTEX B,
457 *Atmos. Chem. Phys.*, 8, 1835-1853, <https://doi.org/10.5194/acp-8-1835-2008>, 2008.
- 458 Pietrogrande, M.C., Bacco, D., Ferrari, S., Kaipainen, J., Ricciardelli, I., Riekkola, M.-L., Trentini,
459 A., and Visentin, M.: Characterization of atmospheric aerosols in the Po valley during the
460 supersito campaigns — Part 3: Contribution of wood combustion to wintertime atmospheric
461 aerosols in Emilia Romagna region (Northern Italy), *Atmos. Environ.*, 122, 291-305,
462 <https://doi.org/10.1016/j.atmosenv.2015.09.059>, 2015
- 463 Pope, C.A., and Dockery, D.W.: Health effects of fine particulate air pollution: lines that connect,
464 *J. Air Waste Manage.*, 56, 709-742, <https://doi.org/10.1080/10473289.2006.10464485>, 2006.
- 465 Sang, X.F., Fu, H.X., Zhang, Y.N., Ding, X., Wang, X.M., Zhou, Y.N., Zou, L.L., Zellmer, G.F.,
466 and Engling, G.: Carbonaceous aerosol emitted from biofuel household stove combustion in
467 South China, *Atmos.*, 11(1), 112, <https://doi.org/10.3390/atmos11010112>, 2020.
- 468 Sang, X.F., Zhang, Z.S., Chan, C.Y., and Engling, G.: Source categories and contribution of
469 biomass smoke to organic aerosol over the southeastern Tibetan plateau, *Atmos. Environ.*, 78,
470 113-123, <https://doi.org/10.1016/j.atmosenv.2012.12.012>, 2013.
- 471 Sang, X.F., Chan, C.Y., Engling, G., Chan, L.Y., Wang, X.M., Zhang, Y.N., Shi, S., Zhang, Z.-S.,
472 Zhang, T., and Hu, M.: Levoglucosan enhancement in ambient aerosol during springtime
473 transport events of biomass burning smoke to Southeast China, *Tellus B* 63, 129-139,
474 <https://doi.org/10.1111/j.1600-0889.2010.00515.x>, 2011.
- 475 Sang, X.F., Gensch, I., Kammer, B., Khan, A., Kleist, E., Laumer, W., Schlag, P., Schmitt, S.H.,
476 Wildt, J., Zhao, R., Mungall, E.L., Abbatt, J.P.D., and Kiendler-Scharr, A.: Chemical stability



- 477 of levoglucosan: An isotopic perspective, *J. Geophys. Res.*, 43, 5419-5424,
478 <https://doi.org/10.1002/2016GL069179>, 2016.
- 479 Schkolnik, G., Falkovich, A.H., Rudich, Y., Maenhaut, W., and Artaxo, P.: New analytical method
480 for the determination of levoglucosan, polyhydroxy compounds, and 2-methylerythritol and
481 its application to smoke and rainwater samples, *Environ. Sci. Technol.*, 39, 2744-2752,
482 <https://doi.org/10.1021/es048363c>, 2005.
- 483 Shen, X.J., Sun, J.Y., Zhang, X.Y., Zhang, Y.M., Wang, Y.Q., Tan, K.Y., Wang, P., Zhang, L., Qi,
484 X.F., Che, H.Z., Zhang, Z., Zhong, J.T., Zhao, H.R., and Ren, S.X.: Comparison of
485 submicron particles at a rural and an urban site in the North China Plain during the December
486 2016 heavy pollution episodes, *J. Meteorol. Res.*, 32, 14-25,
487 <https://doi.org/10.1007/s13351-018-7060-7>, 2018.
- 488 Streets, D.G., Bond, T.C., Carmichael, G.R., Fernandes, S.D., Fu, Q., He, D., Klimont, Z., Nelson,
489 S.M., Tsai, N.Y., Wang, M.Q., Woo, J.H., and Yarber, K.F.: An inventory of gaseous and
490 primary aerosol emissions in Asia in the year 2000, *J. Geophys. Res.*, 108 (D21), 8809.
491 <http://dx.doi.org/10.1029/2002JD003093>, 2003.
- 492 Sullivan, A.P., Holden, A.S., Patterson, L.A., McMeeking, G.R., Kreidenweis, S.M., Malm, W.C.,
493 Hao, W.M., Wold, C.E., and Collett Jr., J.L.: A method for smoke marker measurements and
494 its potential application for determining the contribution of biomass burning from wildfires
495 and prescribed fires to ambient PM_{2.5} organic carbon, *J. Geophys. Res.*, 113, D22302,
496 <https://doi.org/10.1029/2008JD010216>, 2008.
- 497 Sun, K., Liu, X.G., Gu, J.W., Li, Y.P., Qu, Y., An, J.L., Wang, J.L., Zhang, Y.H., Hu, M., Zhang, F.:
498 Chemical characterization of size-resolved aerosols in four seasons and hazy days in the
499 megacity Beijing of China, *J. Environ. Sci.*, 32, 155-167,
500 <https://doi.org/10.1016/j.jes.2014.12.020>, 2015.
- 501 Sun, Y.L., Wang, Z.F., Fu, P.Q., Yang, T., Jiang, Q., Dong, H.B., Li, J., and Jia, J.J.: Aerosol
502 composition, sources and processes during wintertime in Beijing, China, *Atmos. Chem. Phys.*,
503 13, 4577-4592, <https://doi.org/10.5194/acp-13-4577-2013>, 2013.
- 504 Sun, Y.L., Zhang, Q., Anastasio, C., and Sun, J.: Insights into secondary organic aerosol formed
505 via aqueous-phase reactions of phenolic compounds based on high resolution mass
506 spectrometry, *Atmos. Chem. Phys.*, 10, 4809-4822, <https://doi.org/10.5194/acp-10-4809-2010>,
507 2010.
- 508 Tan, J.H., Duan, J.C., Zhen, N.J., He, K.B., and Hao, J.M.: Chemical characteristics and source of
509 size-fractionated atmospheric particle in haze episode in Beijing, *Atmos. Res.*, 167, 24-33,
510 <https://doi.org/10.1016/j.atmosres.2015.06.015>, 2016.
- 511 Tang, R., Wu, Z., Li, X., Wang, Y., Shang, D., Xiao, Y., Li, M., Zeng, L., Wu, Z., Hallquist, M., Hu,
512 M., and Guo, S.: Primary and secondary organic aerosols in summer 2016 in Beijing, *Atmos.*
513 *Chem. Phys.*, 18, 4055-4068, <https://doi.org/10.5194/acp-18-4055-2018>, 2018.
- 514 Urban, R.C., Lima-Souza, M., Caetano-Silva, L., Queiroz, M.E.C., Nogueira, R.F.P., Allen, A.G.,
515 Cardoso, A.A., Held, G., and Campos, M.L. A.M.: Use of levoglucosan, potassium, and
516 water-soluble organic carbon to characterize the origins of biomass-burning aerosols, *Atmos.*
517 *Environ.*, 61, 562-569, <https://doi.org/10.1016/j.atmosenv.2012.07.082>, 2012.
- 518 Wang, Z., Wang, T., Guo, J., Gao, R., Xue, L.K., Zhang, J.M., Zhou, Y., Zhou, X.H., Zhang, Q.Z.,
519 and Wang, W.X., 2012. Formation of secondary organic carbon and cloud impact on
520 carbonaceous aerosols at Mount Tai, North China, *Atmos. Environ.*, 46, 516-527,
521 <https://doi.org/10.1016/j.atmosenv.2011.08.019>, 2012.
- 522 Xu, W., Kuang, Y., Zhao, C., Tao, J., Zhao, G., Bian, Y., Yang, W., Yu, Y., Shen, C., Liang, L.,
523 Zhang, G., Lin, W., and Xu, X.: NH₃-promoted hydrolysis of NO₂ induces explosive growth
524 in HONO, *Atmos. Chem. Phys.*, 19, 10557-10570,
525 <https://doi.org/10.5194/acp-19-10557-2019>, 2019



- 526 Xu, X., Zhang, H., Lin, W., Wang, Y., Xu, W., and Jia, S.: First simultaneous measurements of
527 peroxyacetyl nitrate (PAN) and ozone at Nam Co in the central Tibetan Plateau: impacts from
528 the PBL evolution and transport processes, *Atmos. Chem. Phys.*, 18, 5199–5217,
529 <https://doi.org/10.5194/acp-18-5199-2018>, 2018.
- 530 Yan, C.Q., Zheng, M., Sullivan, A.P., Bosch, C., Desyaterik, Y., Andersson, A., Li, X.Y., Guo, X.
531 S., Zhou, T., Gustafsson, Ö., and Collett, J.L.: Chemical characteristics and light-absorbing
532 property of water-soluble organic carbon in Beijing: Biomass burning contributions, *Atmos.*
533 *Environ.*, 121, 4–12, <https://doi.org/10.1016/j.atmosenv.2015.05.005>, 2015.
- 534 Yan, C.Q., Zheng, M., Sullivan, A.P., Shen, G.F., Chen, Y.J., Wang, S.X., Zhao, B., Cai, S.Y.,
535 Desyaterik, Y., Li, X.Y., Zhou, T., Gustafsson, Ö., and Collett, J.L.: Residential coal
536 combustion as a source of levoglucosan in China, *Environ. Sci. Technol.*, 52(3), 1665–1674,
537 <https://doi.org/10.1021/acs.est.7b05858>, 2017.
- 538 Yang, F.M., Tan, J.H., Zhao, Q. Du, Z.Y., He, K.B., Ma, Y.L., Duan, F.K., Chen, G., and Zhao, Q.:
539 Characteristics of PM_{2.5} speciation in representative megacities and across China, *Atmos.*
540 *Chem. Phys.*, 11, 5207–5219, <https://doi.org/10.5194/acp-11-5207-2011>, 2011.
- 541 Yao, L., Yang, L.X., Chen, J.M., Wang, X.F., Xue, L.K., Li, W.J., Sui, X., Wen, L., Chi, J.W., Zhu,
542 Y.H., Zhang, J.M., Xu, C.H., Zhu, T., and Wang, W.X.: Characteristics of carbonaceous
543 aerosols: Impact of biomass burning and secondary formation in summertime in a rural area
544 of the North China Plain, *Sci. Tot. Environ.*, 557–558,
545 <https://doi.org/10.1016/j.scitotenv.2016.03.111>, 2016.
- 546 Yu, J.T., Yan, C.Q., Liu, Y., Li, X.Y., Zhou, T., and Zheng, M.: Potassium: A Tracer for Biomass
547 Burning in Beijing? *Aerosol Air Qual. Res.*, 18, 2447–2459, doi: 10.4209/aaqr.2017.11.0536,
548 2018.
- 549 Zhang, T., Cao, J.J., Chow, J.C., Shen, Z.X., Ho, K.F., Ho, S.S.H., Liu, S.X., Han, Y.M., Watson,
550 J.G., Wang, G.H., and Huang, R.J.: Characterization and seasonal variations of levoglucosan
551 in fine particulate matter in Xi'an, China, *J. Air Waste Manage.*, 64, 1317–1327,
552 <https://doi.org/10.1080/10962247.2014.944959>, 2014.
- 553 Zhang, T., Claeys, M., Cachier, H., Dong, S.P., Wang, W., Maenhaut, W., and Liu, X.D.:
554 Identification and estimation of the biomass burning contribution to Beijing aerosol using
555 levoglucosan as a molecular marker, *Atmos. Environ.*, 42, 7013–7021,
556 <https://doi.org/10.1016/j.atmosenv.2008.04.050>, 2008.
- 557 Zhang, Z., Engling, G., Lin, C.-Y., Chou, C. C. K., Lung, S.-C. C., Chang, S.-Y., Fan, S., Chan,
558 C.-Y., and Zhang, Y.-H.: Chemical speciation, transport and contribution of biomass burning
559 smoke to ambient aerosol in Guangzhou, a mega city of China, *Atmospheric Environment*, 44,
560 3187–3195, 10.1016/j.atmosenv.2010.05.024, 2010.
- 561 Zhang, Z., Gao, J., Engling, G., Tao, J., Chai, F., Zhang, L., Zhang, R., Sang, X., Chan, C.Y., Lin,
562 Z., and Cao, J.: Characteristics and applications of size-segregated biomass burning tracers in
563 China's Pearl River Delta region, *Atmos. Environ.*, 102, 290–301,
564 <https://doi.org/10.1016/j.atmosenv.2014.12.009>, 2015.
- 565 Zheng, G.J., Duan, F.K., Su, H., Ma, Y.L., Cheng, Y., Zheng, B., Zhang, Q., Huang, T., Kimoto, T.,
566 Chang, D., Pöschl, U., Cheng, Y. F., and He, K. B.: Exploring the severe winter haze in
567 Beijing: the impact of synoptic weather, regional transport and heterogeneous reactions,
568 *Atmos. Chem. Phys.*, 15, 2969–2983, <https://doi.org/10.5194/acp-15-2969-2015>, 2015.
- 569 Zheng, M., Salmon, L. G., Schauer, J. J., Zeng, L., Kiang, C. S., Zhang, Y., and Cass, G. R.:
570 Seasonal trends in PM_{2.5} source contributions in Beijing, China, *Atmos. Environ.*, 39,
571 3967–3976, <https://doi.org/10.1016/j.atmosenv.2005.03.036>, 2005.
- 572 Zhong, J.T., Zhang, X.Y., and Wang, Y.Q.: Reflections on the threshold for PM_{2.5} explosive
573 growth in the cumulative stage of winter heavy aerosol pollution episodes (HPEs) in Beijing,
574 *Tellus B*, 71, 1–7, <https://doi.org/10.1080/16000889.2018.1528134>, 2019.



575 Zhong, J.T., Zhang, X.Y., Wang, Y.Q., Liu, C., and Dong, Y.S.: Heavy aerosol pollution episodes
576 in winter Beijing enhanced by radiative cooling effects of aerosols, *Atmos. Res.*, 209, 59-64,
577 <https://doi.org/10.1016/j.atmosres.2018.03.011>, 2018.

578 Zhou, Y., Xing, X., Lang, J., Chen, D., Cheng, S., Wei, L., Wei, X., and Liu, C.: A comprehensive
579 biomass burning emission inventory with high spatial and temporal resolution in China,
580 *Atmos. Chem. Phys.*, 17, 2839-2864, 10.5194/acp-17-2839-2017, 2017.

581 Zhu, C.S., Cao, J.J., Tsai, C.J., Zhang, Z.S., and Tao, J.: Biomass burning tracers in rural and
582 urban ultrafine particles in Xi'an, China, *Atmos. Pollut. Res.*, 8, 614-618,
583 <https://doi.org/10.1016/j.apr.2016.12.011>, 2017.

584 Zhu, C., Kawamura, K., and Kunwar, B.: Effect of biomass burning over the western North
585 Pacific Rim: wintertime maxima of anhydrosugars in ambient aerosols from Okinawa, *Atmos.*
586 *Chem. Phys.*, 15, 1959-1973, <https://doi.org/10.5194/acp-15-1959-2015>, 2015.

587 Zhu, Y.H., Yang, L.X., Kawamura, K., Chen, J.M., Ono, K., Wang, X.F., Xue, L.K., and Wang,
588 W.X.: Contributions and source identification of biogenic and anthropogenic hydrocarbons to
589 secondary organic aerosols at Mt. Tai in 2014, *Environ. Pollut.*, 220, 863-872,
590 <https://doi.org/10.1016/j.envpol.2016.10.070>, 2017.

591
592
593
594
595
596
597
598
599
600
601
602
603
604
605
606
607
608
609
610
611
612
613
614



615 **Table 1.** Average concentrations and the range of PM_{2.5-cal} and its chemical components, biomass
 616 burning tracers ($\mu\text{g m}^{-3}$), gaseous species, ratios of OC/EC and LG/OC, as well as meteorological
 617 data observed at GC site at daytime, nighttime and whole day, respectively, during the sampling
 618 period from 15 Oct to 23 Nov 2016.

Species	Daytime (N = 34)		Nighttime (N = 33)		Whole period (N = 37)	
	Concentration	Range	Concentration	Range	Concentration	Range
PM _{2.5-cal}	117 ± 58.8	19.0 - 225	170 ± 116	21.1 - 465	137 ± 72.4	23.3 - 319
OC	26.8 ± 15.7	3.78 - 64.8	61.6 ± 49.5	2.88 - 175	44.0 ± 31.0	4.13 - 117
EC	13.4 ± 8.49	1.44 - 34.0	30.9 ± 28.5	2.21 - 129	21.7 ± 15.8	2.46 - 74.9
TC	49.3 ± 27.6	5.76 - 124	92.5 ± 73.6	5.10 - 289	65.8 ± 44.1	7.36 - 192
OC/EC	2.02 ± 1.26	1.09 - 3.31	2.25 ± 1.04	1.04 - 6.72	1.95 ± 0.60	0.83 - 3.10
SO ₄ ²⁻	12.1 ± 9.31	1.65 - 39.7	9.02 ± 6.22	1.55 - 23.2	10.5 ± 6.87	1.66 - 29.5
NO ₃ ⁻	16.9 ± 9.96	1.85 - 41.2	13.1 ± 8.52	1.56 - 38.0	15.9 ± 9.29	2.40 - 45.2
Cl ⁻	4.33 ± 2.30	0.82 - 9.46	6.08 ± 4.00	0.62 - 16.0	4.90 ± 2.46	0.93 - 9.37
NH ₄ ⁺	11.7 ± 6.76	1.84 - 26.0	10.0 ± 5.75	1.33 - 22.2	10.9 ± 5.51	1.99 - 25.4
K ⁺	1.43 ± 0.54	0.20 - 2.64	1.78 ± 0.95	0.22 - 4.19	1.52 ± 0.62	0.50 - 2.96
Mg ²⁺	0.26 ± 0.14	0.07-0.64	0.19 ± 0.09	0.06 - 0.38	0.14 ± 0.12	0.04 - 0.43
Ca ²⁺	2.24 ± 1.01	1.02-4.75	1.56 ± 0.08	0.77 - 3.56	1.54 ± 0.90	0.49 - 3.84
Na ⁺	0.44 ± 0.17	0.10 - 0.79	0.43 ± 0.24	0.10 - 1.31	0.42 ± 0.17	0.11 - 0.88
NO ₃ ⁻ / SO ₄ ²⁻	1.67 ± 0.82	0.75 - 5.52	1.54 ± 0.57	0.74 - 3.50	1.65 ± 0.62	0.78 ± 3.96
Levogluconan	0.57 ± 0.62	0.05 - 3.74	1.10 ± 0.99	0.05 - 4.82	0.79 ± 0.75	0.14 - 4.37
Mannosan	0.024 ± 0.023	0.00 - 0.14	0.05 ± 0.04	0.00 - 0.21	0.03 ± 0.03	0.00 - 0.18
LG/OC	0.018 ± 0.011	0.005 - 0.067	0.020 ± 0.010	0.004 - 0.047	0.020 ± 0.009	0.006 - 0.045
NO (ppb)	23.0 ± 14.7	2.07 - 56.0	45.9 ± 29.5	1.59 - 96.9	31.8 ± 18.3	1.81 - 68.5
NO ₂ (ppb)	25.8 ± 10.4	8.18 - 51.6	29.3 ± 9.37	8.81 - 51.1	26.6 ± 8.74	8.62 - 51.4
SO ₂ (ppb)	9.78 ± 4.96	3.11 - 22.5	9.63 ± 5.67	2.91 - 28.7	8.61 ± 4.04	3.37 - 20.4
CO (ppm)	0.96 ± 0.73	0.03 - 2.49	1.29 ± 1.04	0.02 - 3.26	1.05 ± 0.76	0.12 - 2.48
O ₃ (ppb)	13.0 ± 9.10	1.42 - 41.84	5.00 ± 5.73	1.60 - 24.30	9.25 ± 5.78	1.67 - 24.0
NH ₃ (ppb)	16.4 ± 11.3	1.68 - 46.2	18.3 ± 10.7	1.03 - 42.7	17.1 ± 9.88	1.46 - 44.4
Temperature (°C)	7.71 ± 4.01	- 2.07-15.9	3.30 ± 4.69	- 6.60 - 14.5	6.95 ± 4.58	- 4.33 - 15.4
Relative Humidity (%)	68 ± 17	31 - 98	85 ± 14	34 - 100	77 ± 13	48 - 99
Wind speed (m s ⁻¹)	1.43 ± 1.17	0.09 - 5.65	0.79 ± 1.55	0.03 - 7.19	1.07 ± 1.14	0.04 - 5.02

619
 620
 621
 622
 623
 624
 625
 626



627 **Table 2.** Concentrations of chemical components in PM_{2.5} aerosols as well as their ratios and
 628 gaseous species collected at the GC site, during the four biomass burning periods (i.e., Minor,
 629 Intensive, Major and Heating period) from 15 Oct to 23 Nov 2016.

Species	Period I (15-30 Oct)	Period II (31 Oct)	Period III (1 -14, Nov)		Period IV (15 -23, Nov)		
	Minor BB Concentration	Intensive BB Concentration	Ratio*	Major BB Concentration	Ratio*	Heating period Concentration	Ratio*
PM _{2.5-cal}	81.0 ± 44.5	235	2.91	163 ± 46.7	2.01	189 ± 83.0	2.33
Levogluconan	0.36 ± 0.14	4.37	12.1	0.90 ± 0.37	2.50	0.96 ± 0.63	2.67
Mannosan	0.015 ± 0.005	0.18	12.0	0.038 ± 0.015	2.53	0.050 ± 0.026	3.33
OC	16.2 ± 7.52	96.3	5.93	55.2 ± 17.1	3.41	69.4 ± 24.6	4.28
EC	12.2 ± 5.85	36.0	2.96	25.5 ± 10.1	2.09	36.4 ± 21.5	2.98
TC	28.4 ± 13.1	132	4.66	80.9 ± 34.6	2.85	106 ± 55.3	3.73
SO ₄ ²⁻	10.3 ± 8.96	4.56	0.44	11.8 ± 6.02	1.15	9.08 ± 3.87	0.88
NO ₃ ⁻	16.6 ± 12.9	18.1	1.09	16.5 ± 6.42	0.99	12.6 ± 5.76	0.76
NH ₄ ⁺	10.1 ± 7.40	10.0	0.99	12.0 ± 4.35	1.19	10.3 ± 3.62	1.02
K ⁺	1.16 ± 0.36	2.61	2.25	1.76 ± 0.46	1.52	1.65 ± 0.84	1.42
Cl ⁻	3.46 ± 1.97	7.49	2.16	5.58 ± 2.16	1.61	6.27 ± 2.58	1.81
OC/EC	1.53 ± 0.35	2.67	1.75	2.31 ± 0.59	1.51	2.04 ± 0.31	1.33
NO ₃ ⁻ /SO ₄ ²⁻	1.74 ± 0.60	3.96	2.28	1.50 ± 0.35	0.86	1.42 ± 0.47	0.82
LG/OC	0.025 ± 0.008	0.045	1.80	0.016 ± 0.005	0.64	0.014 ± 0.006	0.56
LG/EC	0.039 ± 0.019	0.121	3.10	0.038 ± 0.017	0.97	0.028 ± 0.013	0.72
LG/MN	24.9 ± 4.44	24.1	0.97	24.8 ± 6.46	1.00	18.3 ± 4.27	0.73
LG/K ⁺	0.36 ± 0.081	1.67	4.64	0.51 ± 0.16	1.42	0.53 ± 0.15	1.47
NO (ppb)	21.7 ± 12.5	21.7	1.00	39.6 ± 15.4	1.82	39.3 ± 23.6	1.81
NO ₂ (ppb)	21.8 ± 4.95	26.5	1.22	32.7 ± 7.27	1.50	24.6 ± 10.2	1.13
NO _x (ppb)	43.6 ± 16.3	48.2	1.11	72.4 ± 17.8	1.66	64.0 ± 33.4	1.47
SO ₂ (ppb)	5.83 ± 2.46	8.04	1.38	11.1 ± 4.10	1.90	9.75 ± 3.31	1.67
CO (ppm)	0.44 ± 0.33	0.70	1.59	1.65 ± 0.53	3.75	1.18 ± 0.83	2.68
O ₃ (ppb)	9.79 ± 4.88	23.2	2.37	7.51 ± 3.87	0.77	9.59 ± 7.55	0.98
NH ₃ (ppb)	14.3 ± 6.12	11.1	0.78	18.6 ± 8.03	1.30	21.2 ± 14.2	1.48

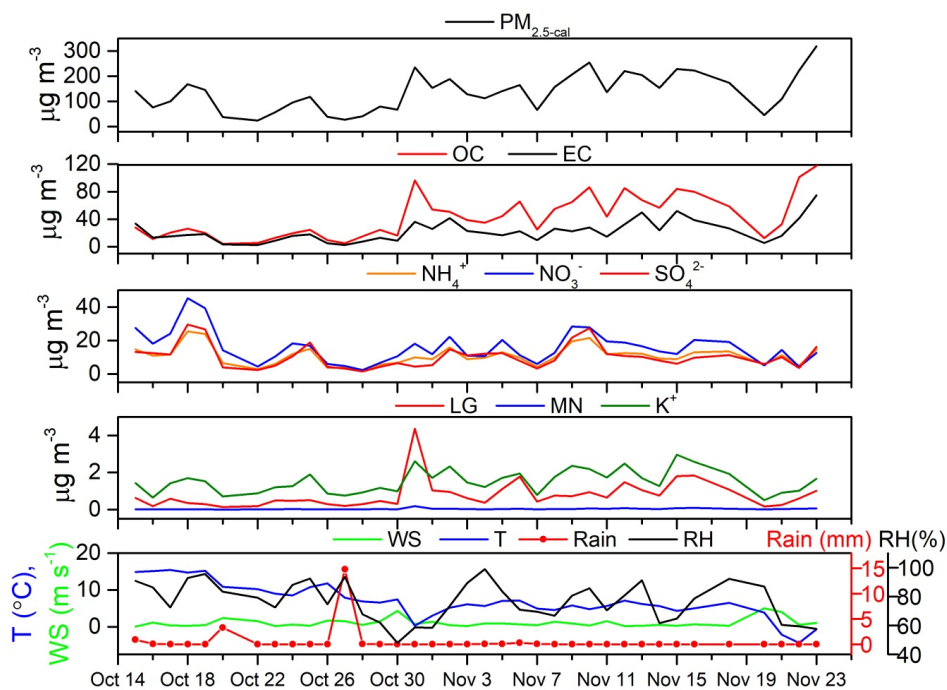
630 *: indicates that the ratios of the heating period, intense BB period or major biomass burning period
 631 were divided by those from the minor BB period.

632

633

634

635



6

637 **Figure 1.** Time-series variation obtained for $PM_{2.5-cal}$ and its major components (OC, EC, SO_4^{2-} ,
638 NO_3^- and NH_4^+), biomass burning tracers (LG, MN and K^+) and meteorological factors
639 (temperature (T), relative humidity (RH), wind speed (WS) and rainfall) at the GC site during the
640 sampling period from 15 Oct to 23 Nov 2016.

641

642

643

644

645

646

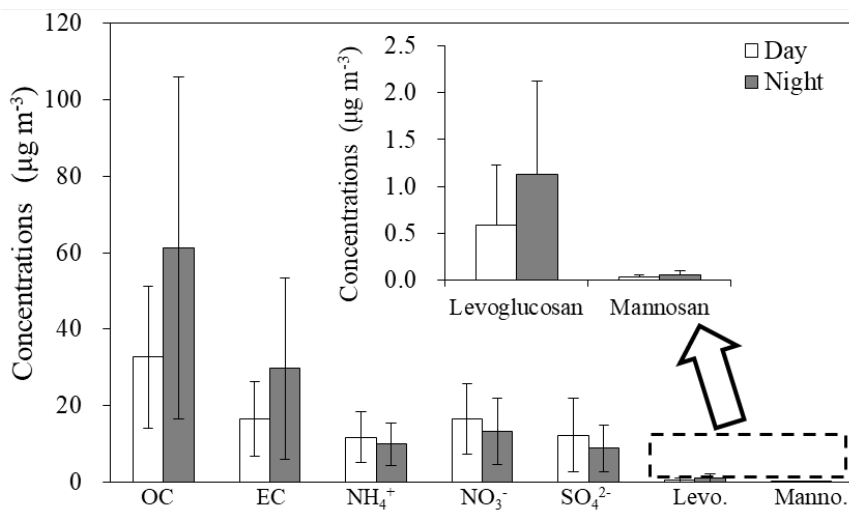
647

648

649

650

651



652

653

654

655

Figure 2. Day and night distributions of mean concentrations of main chemical components (OC, EC, SO₄²⁻, NO₃⁻ and NH₄⁺) and biomass burning tracers (LG and MN) in PM_{2.5} observed at GC site during the sampling period.

656

657

658

659

660

661

662

663

664

665

666

667

668

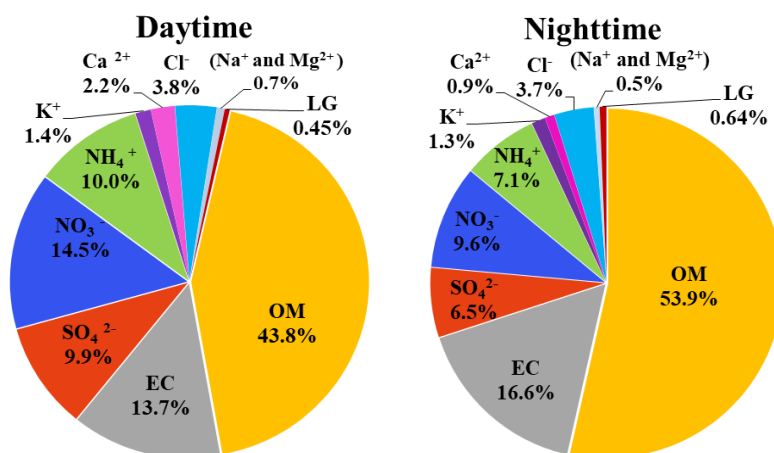
669

670

671

672

673



674

675 **Figure 3.** Percent contributions of individual component mass concentrations to total estimated

676 PM_{2.5-cal} mass in daytime and nighttime during the sampling period.

677

678

679

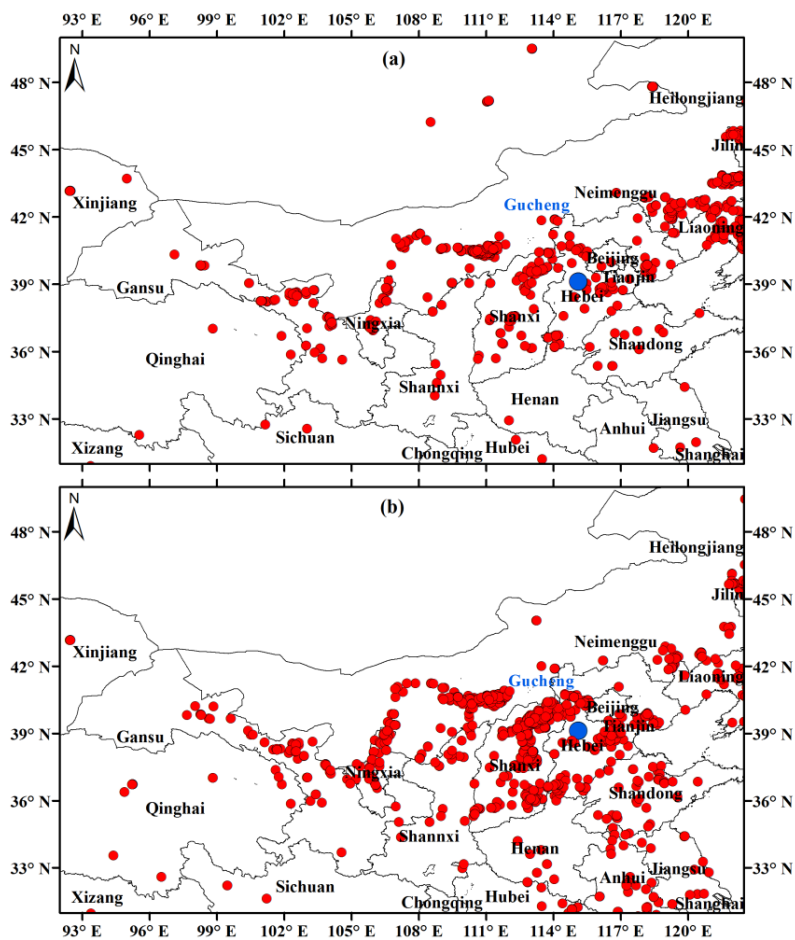
680

681

682

683

684



685

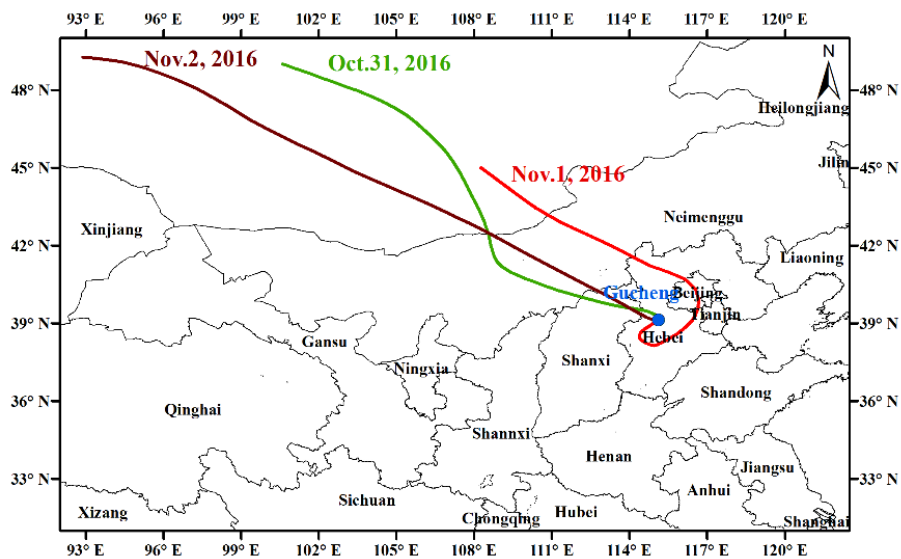
686 **Figure 4.** Fire spots at GC site and the surrounding provinces from (a) 15-30 October, 2016 and (b)
687 1 -23, November, 2016, observed by MODIS Terra satellites (blue dot is GC station).

688

689

690

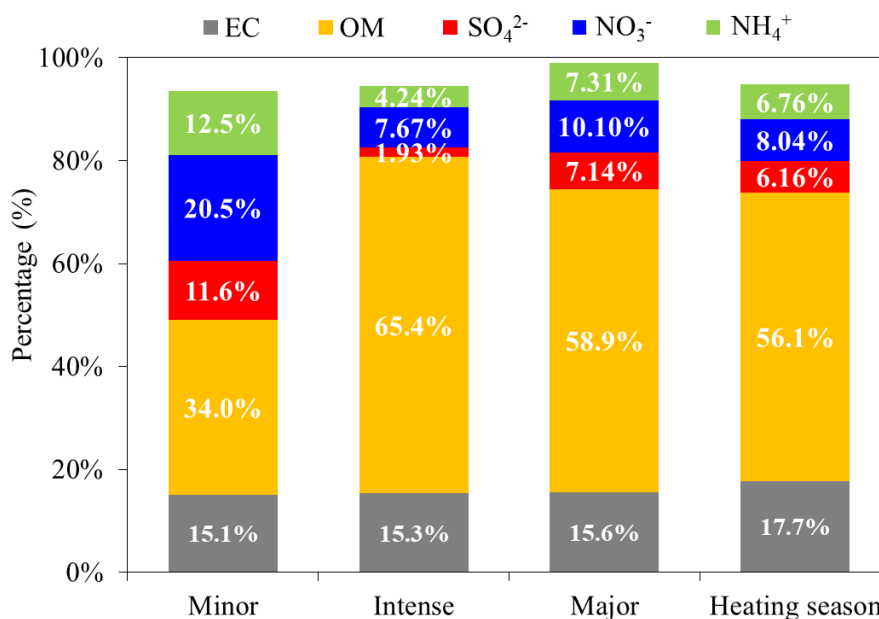
691



692
693

694 **Figure 5.** 48 h back trajectories at 500 m at GC site (39°09'N, 115°44'E) at 00:00 (UTC time)
695 from 31 October to 2 November, 2016.

696
697
698
699
700
701
702
703
704
705
706
707



708

709 **Figure 6.** Mean percentiles of major components in PM_{2.5} with respect to different biomass
710 burning pollution periods at GC site during the sampling time.

711

712

713

714

715

716

717

718

719

720

721

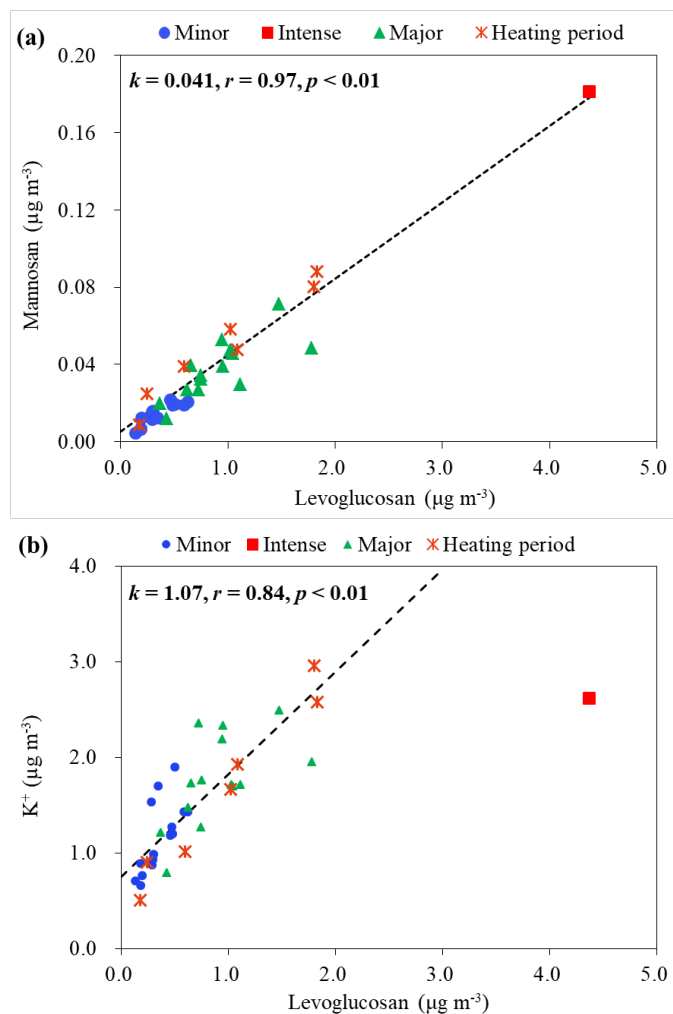
722

723

724

725

726



727

728

729

Figure 7. Scatter plots of (a) levoglucosan versus mannosan, (b) levoglucosan versus K^+ .

730

731

732

733

734

735

736

737

738